ACS APPLIED MATERIALS & INTERFACES

Research Article

www.acsami.org

Multifunctional Composite Coating as a Wear-Resistant Layer for the Bearing in Total Hip Joint Replacement

Seung Mok Cho,[†,‡,§] Jin-Woo Park,[*,‡] Hyung-Seop Han,[†] Hyun-Kwang Seok,[†] Myoung-Woon Moon,[⊥] and Yu Chan Kim[*,†]

[†]Biomedical Research Institute, [⊥]Future Convergence Research Division, Korea Institute of Science & Technology (KIST), Seoul 136-650, Korea

[‡]Department of Materials Science and Engineering, Yonsei University, Seoul 120-749, Korea

Supporting Information

ABSTRACT: In this study, we developed Ti-TiN composite coatings with fine lamellar structures for use as an enhanced wear-resistant layer between the bearing components of the polymer-lined acetabular cup and the metal femoral head of total hip joint replacements (THRs). A plasma spraying deposition method was used to apply the composite coatings, and the thickness of TiN layer in the composite could be controlled by varying the flow rate of N_2 atmospheric gas. The surface properties, such as roughness and hardness, were analyzed, and the friction coefficient (μ) and wear rate (k) were measured using a bovine serum wear test. A biocompatibility test was performed to evaluate the toxicity of the composite coatings. Our experimental results reveal that the friction and wear resistance of composite coatings is superior to that of the metallic implant materials, and they have a higher level of fracture toughness as compared with other ceramic coatings because of a good balance between the hardness of the TiN and the toughness of the Ti. Furthermore, these coatings possessed excellent biocompatibility. The experimental results also demonstrate that the improved wear properties can be attributed to a certain level of unavoidable porosity that is due to the rapid solidification of liquid droplets during the plasma spraying process. The pores in the coating surface play an important role as a lubricant (bovine serum) reservoir, reducing the actual contact area and friction losses.

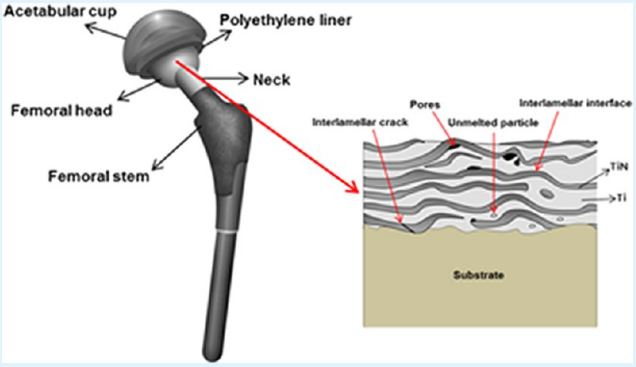

KEYWORDS: *hip replacement prosthesis, biotribology, composite coatings, biocompatibility*

1. INTRODUCTION

As the human lifespan has been significantly extended by the considerable advancements in medical technology, the short lifespan of implanted prosthetics has become one of the most critical issues in the use of joint replacements.[1] The longevity of total hip joint replacements (THRs) was expected to be approximately 15 years for patients who received the surgery before the age of 65.[1] However, with lengthening of the human lifespan and the increasing number of younger patients who are traumatized by sports and accidents, multiple revision surgeries are increasingly required, which are not only expensive but have a low success rate.[2]

THRs consist of a polymer-lined acetabular cup, a metallic femoral head, and a stem, as schematically depicted in Figure 1. Of these components, the polymer liner and metal head comprise a bearing couple for the prosthesis, and the friction and wear properties of the bearing are critical factors in the longevity of the implant.[1,3] The release of very small particles of wear debris from the bearing over a long period of time may cause osteolysis and inflammatory reactions.[1] In addition, generation of this debris can ultimately result in the loosening and eventual failure of the implant.[4]

Biotribology encompasses the study of the articulation of the artificial bearing under applied loads and motion that is characterized by three factors: the wear, friction, and lubrication on the two mated surfaces.[5] Minimizing the contact between the two articulating surfaces by full fluid film lubrication is essential; otherwise, the friction between the surfaces will increase, producing a greater amount of wear debris.[5] The friction on the bearing surfaces directly affects the stresses transmitted through the fixation interface.[6] Therefore, to reduce the frictional force transmitted to the fixation interface between the acetabular cup and the femoral head in hip joint replacements, it is important to minimize the friction coefficient (μ).[7]

Received: October 25, 2012
Accepted: December 18, 2012
Published: December 18, 2012

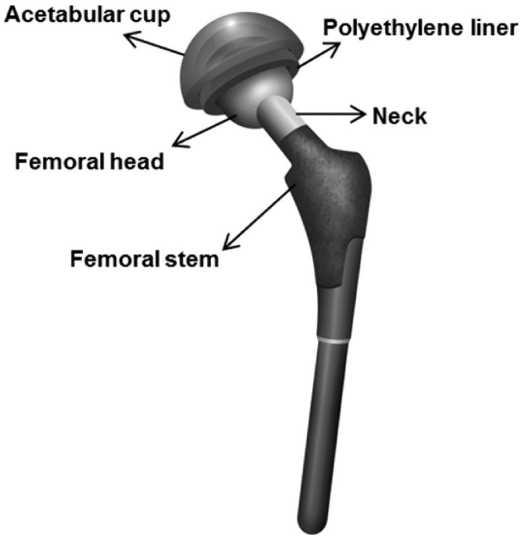

Figure 1. Schematic description of the THRs.

The wear volume is proportional to the normal load and the sliding distance, and the wear rate (k), the proportionality constant, represents the wear resistance of the materials.[7] In general, low friction does not always imply low wear, and vice versa.[8] However, the wear and friction resistances and the effect of the lubrication usually depend on the surface properties of the contact areas of the bearing, such as surface roughness (R_{rms}), hardness, and the wettability of the lubricant.[6,8] It has been reported that polymeric materials wear less on a smoother metal than on a rougher one, and hard ceramics are better counterparts than metals in terms of wear.[9]

The most widely used material for the polymer liner is ultrahigh-molecular-weight polyethylene (UHMWPE) because it exhibits a small k, high mechanical strength, and biocompatibility.[10] The metallic materials used most extensively for the femoral head have been 316L stainless steels, Co−Cr alloys, and Ti and its alloys.[1] The Co−Cr alloys are known for their superior wear resistance, but Co and Cr ions released as a result of corrosion in the body environment may cause cytotoxicity.[1,4] Ni debris from stainless steels has also been reported to cause skin-related diseases, such as dermatitis.[1]

Ti and Ti-6Al-4 V are the most commonly used Ti-based materials for implant applications because they possess high strength per density (specific strength), high corrosion resistance, and excellent biocompatibility.[11] In these areas, the Ti-alloys are known to outperform any other implant metals; however, their large μ and poor wear resistance result in the generation of wear particles, causing pain and loosening of the THRs.[1] To overcome the drawbacks of the current metallic implant materials, the metal surfaces have been coated with hard ceramic materials, such as diamond-like carbon (DLC), TiN, or Ti oxides.[9,12] When the ceramic coating is thick enough, it can protect the metal surface against wear from third body particles.[13] However, residual stress is induced in the coating during its deposition as a result of the large differences in thermo-mechanical properties between the metallic part and the ceramic coating. Because of the low toughness of the ceramic, this stress leads to brittle fracture of the ceramic coating, which limits the long-term clinical use of the coating.[1,14]

In this study, a composite coating was designed to overcome the drawbacks of the previously developed coating materials. By hybridization of the metal and the ceramic, materials having both the hardness of the ceramic and toughness of the metal can be made. A reactive plasma spraying method was selected to deposit the composite coatings. The plasma spraying process is known to be a reliable and cost-effective technique for depositing structural and functional coatings of various materials on a wide range of substrates.[15] The coating was Ti-based, but a Ti-TiN laminate composite was eventually formed by controlling the atmospheric gases during the plasma spraying process. Three types of composite coatings were produced at different N_2 flow rates. The surface properties of the coatings were analyzed, and the friction and wear resistances of the coatings against the UHMWPE were also measured and compared with those of Co−Cr alloys. To simulate clinical testing conditions, we used bovine serum as a lubricant; we also tested the biocompatibility of the coatings.

2. EXPERIMENTAL PROCEDURES

2.1. Sample Preparations. Three different coatings were deposited via plasma spraying on 304 stainless steel (SUS304) for the surface and microstructural analyses, and the wear test. For the biocompatibility test, Ti-6Al-4 V alloy substrates were used. Nontoxic Ti powders (99.95%, LTS Chemical, Inc.) with an average particle size of approximately 35−43 μm (−325 mesh) were sprayed under a controlled atmosphere of either Ar (99.999%) or N_2 (99.999%) gas in a spraying chamber. During plasma spraying, the flow rate of N_2 gas in the chamber was controlled at 25 and 1000 L/min. The different processing conditions are summarized in Table 1. Prior to plasma spraying, the Ti powders were dried at 80 °C for 30 min in a forced convection oven. Sand-blasting of the substrate surface was performed prior to plasma spraying to enhance coating adhesion. To compare the wear properties of the coatings with Co−Cr alloys, we produced the Co-28Cr-6Mo alloy, which is used most extensively, via arc melting.

2.2. Structural Characterization. The shape and surface morphology of the Ti powders were analyzed using scanning electron microscopy (SEM). The phase compositions of the Ti powders and coatings were analyzed using X-ray diffraction (XRD) analysis. The XRD analysis was performed in the range of 20−80° in the 2θ mode. The microstructures of the coating surfaces and coating cross sections were analyzed using field emission scanning electron microscopy (FE-SEM). Chemical analysis was performed using a field emission gun electron probe microanalyzer (FEG-EPMA) with a backscattered electron (BSE) mode and Auger electron spectroscopy (AES). The interfacial microstructures between Ti and TiN in the coatings were analyzed using high-resolution transmission electron microscopy (HR-TEM). The TEM specimens were prepared using a focused ion beam (FIB).

2.3. Surface Analysis and Mechanical Tests. The surfaces of the three coatings and the Co-28Cr-6Mo alloy were ground and polished prior to the surface analysis and the wear tests. The surface

Table 1. Types of Coatings and the Processing Conditions for Plasma Spraying

type	atmospheric gas	atmospheric gas flow rate (L/min)	current (A)	plasma gas, Ar (L/min)	plasma gas, He (L/min)	spraying distance (mm)	chamber vacuum (torr)
1	Ar	1000	600	36	20	120	1×10^{-2}
2	N_2	25					
3	N_2	1000					

dx.doi.org/10.1021/am302452f | ACS Appl. Mater. Interfaces 2013, 5, 395−403

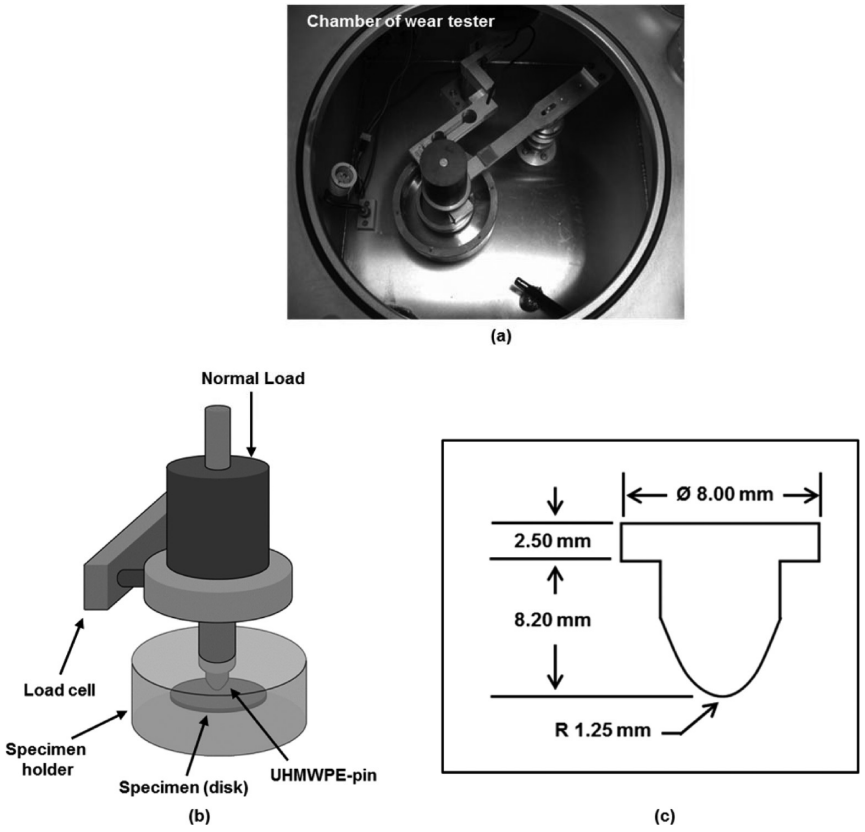

Figure 2. (a) Wear tester chamber; (b) schematic descriptions of the wear tester: the chamber, pin, and disc; (c) the dimensions of the UHMWPE pin.[16].

Table 2. Surface Roughness (R_{rms}), Contact Angle (θ), Friction Coefficient (μ), and Wear Rate (k) of the Three Coatings and the Co−Cr−Mo Alloys ((StDev*) is the standard deviation)

samples	R_{rms} (nm)	hardness (StDev*) (Hv)	θ (deg)	μ (StDev*)	k ($\times 10^{-15}$ kg/Nm) (StDev*)
Co-28Cr-6Mo	3.0	365.6 (26.7)	73.8	0.027 (0.002)	21.2 (1.8)
Type 1	15.5	270.1 (28.1)	64.1	0.028 (0.001)	24.6 (2.4)
Type 2	51.9	756.4 (162.8)	63.6	0.035 (0.001)	18.3 (2.2)
Type 3	476.5	1098.5 (214.3)	61.4	0.041 (0.002)	16.7 (2.3)

roughness (R_{rms}) was measured using atomic force microscopy (AFM). Coating hardness was measured using the micro-Vickers hardness test under the 100 gf loading condition. The hardness was measured at more than 10 randomly selected points on the surface. The values of μ and k were measured using the pin-on-disk type wear tester that is schematically depicted in Figure 2a−c.[16]

To simulate clinical testing conditions, 0.2-μm-filtered bovine serum (GIBCO, Invitrogen Corporation) was used as a lubricant. The lubricant was diluted with distilled water up to 75% in volume fraction, and the serum contained a mass fraction of 0.2 sodium azide (Sigma-Aldrich) to minimize bacterial degradation. Ethylene-diaminetetracetic acid (EDTA, Sigma-Aldrich) was added to the serum at a concentration of 20 mM (7.45 g/L) to bind Ca^{2+} ions present in the solution and to minimize the precipitation of abrasives onto the bearing surfaces. Prior to the wear test, the wettability of the lubricant on the Co-28Cr-6Mo alloy and Ti-based coatings (Table 1) was tested by contact angle measurement.

The pin in Figure 2b is the UHMWPE, and the disk (diameter, 3 cm; height, 1 cm) is either one of the three Ti-based coatings on the SUS304 substrate, as listed in Table 1, or the Co-28Cr-6Mo alloy without a coating. The shape of the UHMWPE pin is shown in detail in Figure 2c.[16] The UHMWPE pin was soaked in distilled water for 2 weeks prior to the test to reduce error in measurements for the net increase in weight or volume during the initial wear intervals due to fluid sorption.[16] The chamber temperature was maintained at 36−38 °C during the test, and distilled water was added as needed to replace water losses due to evaporation.

UHWMPE wear was measured after 216 000 cycles at 2.5 Hz with a contact force of 26.5 N. The total sliding distance was 10.17 km. UHMWPE wear loss was determined by weighing the component on a microbalance (Mettler Toledo, AX106) after running the test for 10 h. The weight of the tested UHMWPE was then measured after drying for one day to reduce error. The same experiment was repeated three times, and the results for k are presented as an average in Table 2.

2.4. Biocompatibility. The biocompatibility of Type 1 and 3 coatings on Ti-6Al-4 V alloy discs (diameter, 1 cm; height, 0.3 cm) was tested following ISO standards ISO10993−1[17] and ISO10993−5.[18] A mouse embryonic fibroblast cell line (NIH 3T3) was cultured in a medium of Dulbecco's modified eagle medium (DMEM)-10% fetal bovine serum (FBS). The HeLA cells were separated from the culture medium using 0.025% Trypsin/EDTA and centrifugation. An initial quantity of 1×10^4 cells was placed on the coatings to evaluate the biocompatibility and cytotoxicity of the coatings in terms of the degree of cell growth after 48 h.

3. RESULTS

3.1. Microstructures of Ti-Based Composite Coatings. The SEM image in Figure 3a shows the irregular shapes of the Ti powders, and the XRD analysis results in Figure 3b reveal

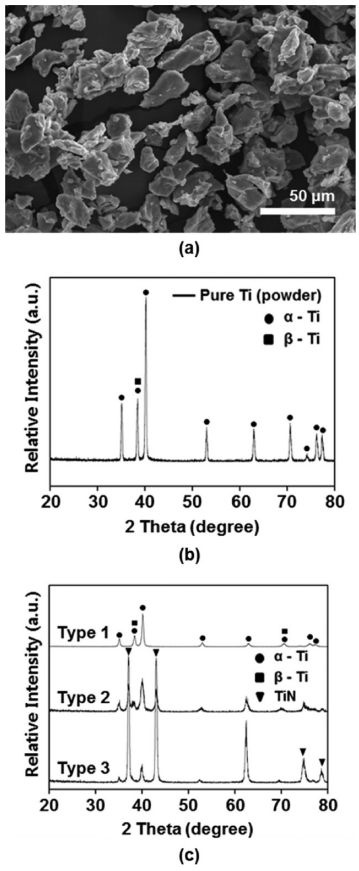

Figure 3. (a) SEM image of the Ti powders, (b) XRD result of the Ti powders, (c) XRD result of the plasma-sprayed coatings.

that the Ti powders are mostly α-Ti, but the β-Ti phase is also present. Figure 3c shows the results of the XRD analyses of the three different coatings described in Table 1. According to Figure 3c, Type 1 is mostly crystalline α-Ti, similar to the Ti powders, and Types 2 and 3 have both crystalline α-Ti and TiN peaks. In particular, the intensity of the TiN peaks is strongly enhanced in Type 3 as compared with Type 2, which demonstrates that the thickness of TiN layer in the composite can be controlled by adjusting the amount of N_2 gas when other deposition conditions are fixed (Table 1).

Figure 4a–f show FE-SEM normal and backscattered electron (BSE) images that depict the cross-sectional microstructures and surface morphologies of the three types of coatings. As shown in Figure 4a–c, the average thicknesses of the three coatings are 180–200 μm. In Figure 4, two important microstructural characteristics should be noted: (1) under an N_2 atmosphere, lamellar structures are formed with alternating Ti and TiN layers; (2) Type 2 and 3 coatings are porous as compared with the Type 1 coating, and the pore density increases as the N_2 flow rate increases. The lamellar structures in the coatings were verified by the AES and EPMA elemental mapping results shown in Figures 5 and 6, respectively.

The AES results in Figure 5a indicate that the thicknesses of the Ti and TiN layers in the lamellar structures of Type 2 are similar at approximately 2–5 μm. In Type 3, the thickness of the TiN layer is significantly increased to 10–20 μm (Figure 5b). The Ti layer in Type 3 is not as continuous as in Type 2 and seems to be embedded in the TiN layer. Figure 5b also shows that more pores and cracks are present in Type 3 than in Type 2. On the top surfaces of the coatings, similar microstructural characteristics to the cross sections are observed. Panels a and b in Figure 6 confirm that Type 2 has finer lamellar structures and is less porous than Type 3. In most previously reported cases, titanium-nitride coatings applied using plasma spraying formed a coating layer with a small amount of a titanium-oxide phase. Notably, in the AES and EPMA results, small oxides are formed in the coatings.

Figure 7a shows the HR-TEM bright-field image and selected area diffraction patterns (SADPs) of the interface and the adjacent materials of the Type 2 coating. According to Figure 7a, a sound interface with few defects is formed between the polycrystalline TiN (region A) and the polycrystalline Ti (region B). Images b and c in Figure 7 depict the HR-TEM images of the nanostructured TiN phases in Types 2 and 3, respectively. The rapid cooling during the plasma spraying

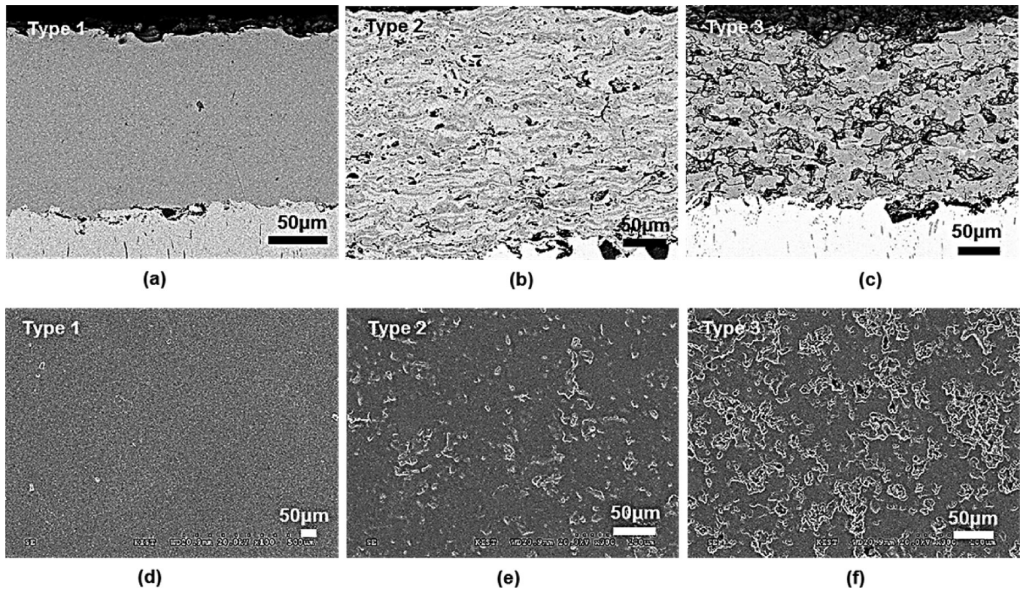

Figure 4. (a–c) FE-SEM images of the cross-sectional images of Type 1–3 coatings, (d–f) FE-SEM surface images of Types 1–3 coatings.

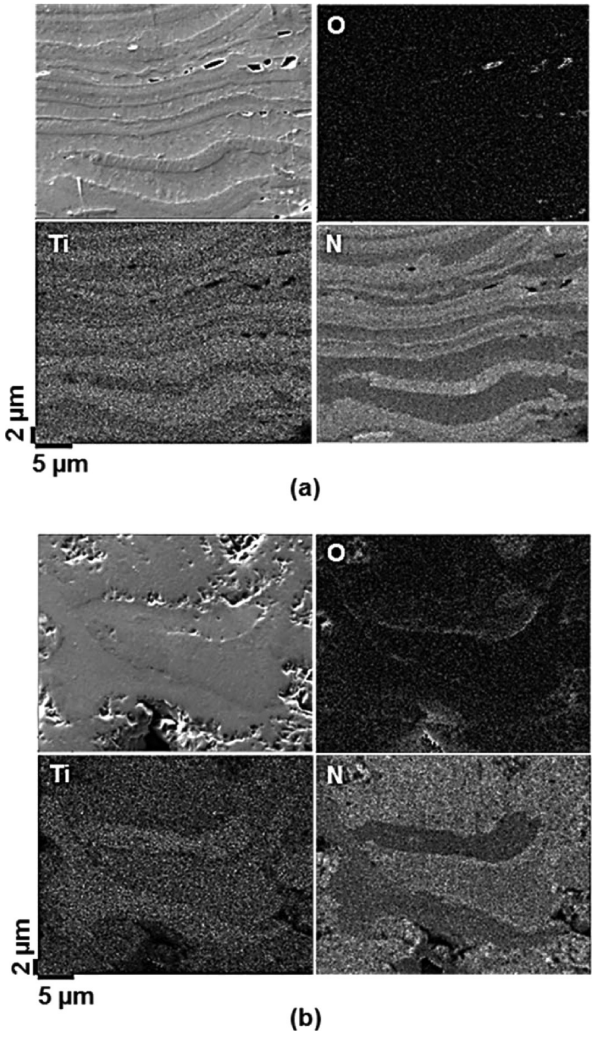

Figure 5. AES element mapping results of the cross sections of (a) Type 2 and (b) Type 3 coatings.

process resulted in the nanosized grains observed in the coatings.

3.2. Surface and Mechanical Properties of the Composite Coatings. The surface properties of the three coatings are summarized and compared with those of the Co-28Cr-6Mo alloys in Table 2. According to the measured results reported in Table 2, the R_{rms} values of Types 1−3 are greater than the R_{rms} value of the Co-28Cr-6Mo alloy. In particular, the R_{rms} values of Types 2 and 3 are two to 3 orders of magnitude larger than the R_{rms} value of the Co-28Cr-6Mo alloy due to the high pore density, as shown in Figure 4. As reported in Table 2, the hardness is greatly enhanced in the composite coatings as compared with the Co-28Cr-6Mo alloy and Type 1 coating, and hardness increases as the thickness of TiN layer in the coating increases. However, the coating hardness standard deviations for Types 2 and 3 are also greater than those of the other two samples because of their lamellar structure and inhomogeneous pore distributions.

According to Table 2, the values of θ measured for Types 1−3 are smaller than that measured for the Co-28Cr-6Mo alloy, but there is a negligible difference among the θ values of the three coatings. The value of θ is a function of the surface area as well as the surface energy.[19] Because coating Types 1−3 are more porous than the Co-28Cr-6Mo alloy, as shown in Figures 4−6, the effective surface area that contacts the lubricant is increased. Based on these results and the results in Table 2, the coating surfaces of Types 1−3 appear to be more hydrophilic than the Co-28Cr-6Mo alloy because of the pores on their surfaces.

The wear test results (μ and k) are compared in Figure 8 and Table 2. Figure 8 presents the observed variations in μ as the sliding distance increases, and the average μ values are summarized in Table 2. According to Figure 8, the μ values of Types 2 and 3 are higher than those observed for the Co-28Cr-6Mo alloy and Type 1 throughout the applied sliding distance. In particular, the μ value of Type 3 is the highest among the tested samples and is larger than the μ value of the Co−Cr alloy by more than 35% (Table 2). Although the μ values of the Co-28Cr-6Mo alloy and Type 1 increased to 1000 m and then remained almost constant until the end of the test, the μ values of Types 2 and 3 slightly decreased as the sliding distance increased.

As shown in Table 2, the wear properties of the composite coatings (Types 2 and 3) are greatly enhanced as compared with those of the Co-28Cr-6Mo alloy and Type 1 coating. The value of k for Type 3 is the smallest among the samples and is approximately 25% smaller than the value of k for the Co-28Cr-6Mo alloy. A comparison of the three coatings, Types 1−3, reveals that k is inversely proportional to μ and decreases as the thickness of TiN layer increases although the pore density increases with this thickness.

3.3. Biocompatibility. The biocompatibility test results for coating Types 1 and 3 are summarized in Figure 9. The survival rates of the HeLa cells on Types 1 and 3 were higher than the control as presented in Figure 9, which indicates excellent biocompatibility with no toxicity from the coatings. Type 1 shows a slight increase of cell viability when compared to the 100% control, whereas there was a significant increase of the cell viability in 48 h.

4. DISCUSSION

In this study, we successfully developed Ti-TiN composite coatings with fine lamellar structures using reactive plasma spraying with atmospheric control. The plasma generated by high-voltage electrodes creates partially or fully melted Ti particles (droplets) that traverse the plasma jet. The nitride reaction occurs on the surface of the droplets during flight to the substrate under an N_2 atmosphere. Ti droplets with TiN on the surface are deposited on the substrate in a flattened shape, and they rapidly solidify to form an interlocking lamellae (or splats) structure. Figure 10 schematically depicts the plasma spraying and deposition processes.

One of the most beneficial properties of the composite coatings is that a compromise between hardness and toughness can be achieved. Using the plasma spraying process developed in this study, the mechanical properties of the coating can be tailored by varying the thickness of TiN layer, which is controlled by the N_2 flow rate. As mentioned previously, ceramic coatings have enhanced hardness and wear properties as compared with metal implant materials, but the brittleness of the ceramics limits the application of the coatings. The improved fracture toughness of the composite coatings was also verified in that no fracture and delamination between the coating and the substrate was observed after the wear test.

In real systems involving the accumulation of many solidifying droplets, porosity is an inherent problem and is believed to reduce useful properties such as strength and

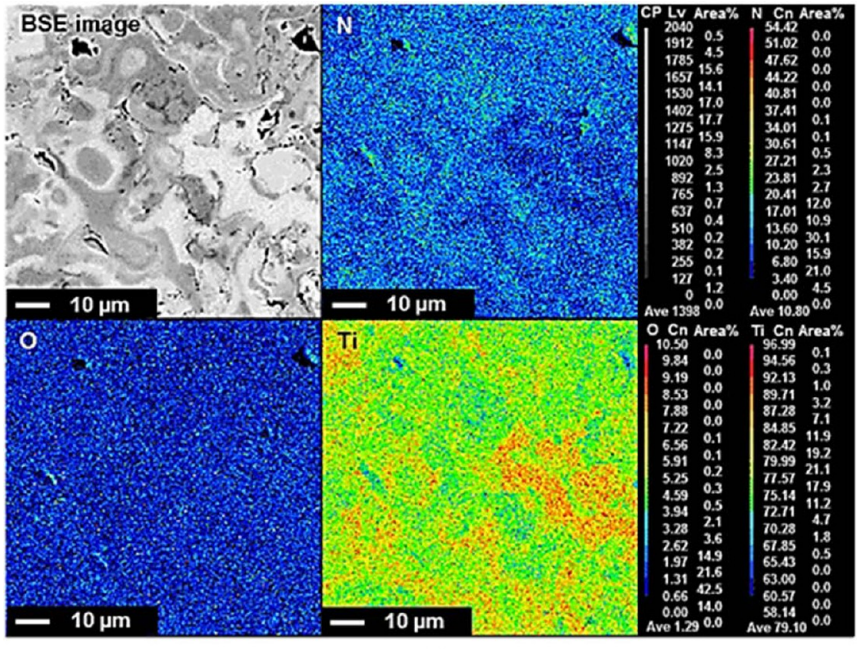

(a)

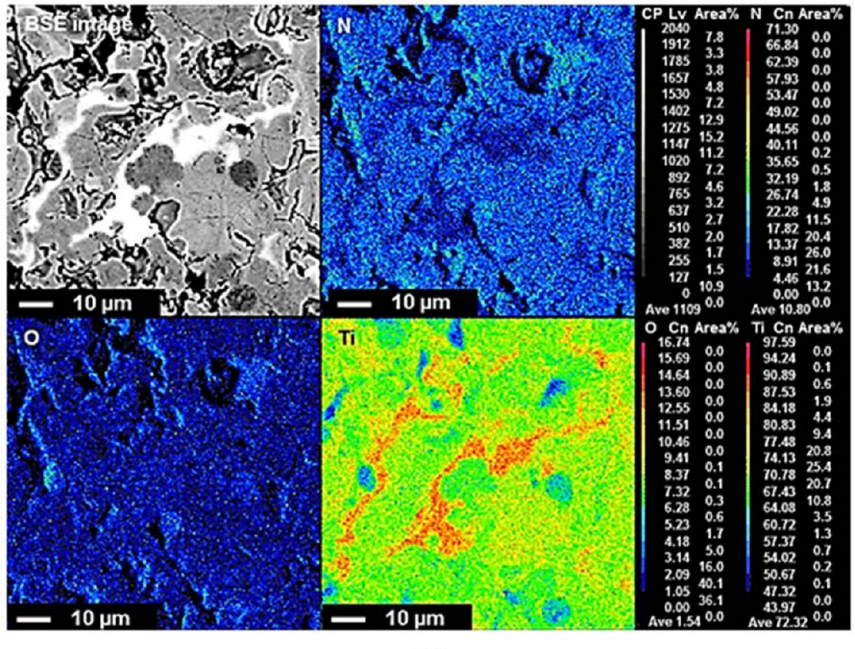

(b)

Figure 6. EPMA (element mapping) results from surface analysis for (a) Type 2 and (a) Type 3 coatings.

corrosion resistance.[20] The pore density is reduced because the liquid droplets have greater energy to penetrate into the pores. Their energy increases with velocity and droplet density.[20] On the basis of the results presented in Figures 4−6, the coatings become more porous as the thickness of TiN layer increases although TiN has a greater density than Ti. This result occurs because the TiN formed on the outer surface of the flying droplets is almost solid because of the high melting point of TiN. As thick TiN is formed on the surface, the impinged droplets are too stiff to penetrate into the pores.

However, the Type 3 coating, which is the most porous and thus has the roughest surface, was found to have the best wear properties against the UHMWPE among the tested samples. UHMWPE wear depends not only on the surface roughness of the counterpart materials but also on the relationship between the lubricant and the pores.[21] The positive effects of the pores in coating Types 2 and 3 on the wear of UHMWPE are as follows: (1) the pores and cavities can act as bovine serum reservoirs, which prevent dry running at the start of the test and reduce the actual contact area and friction losses;[22] and (2) as the metal surface becomes rougher, the temperature of the contact areas during the wear test can increase. This increased temperature may cause denatured proteins from the bovine serum to accumulate more rapidly between the UHMWPE-pin

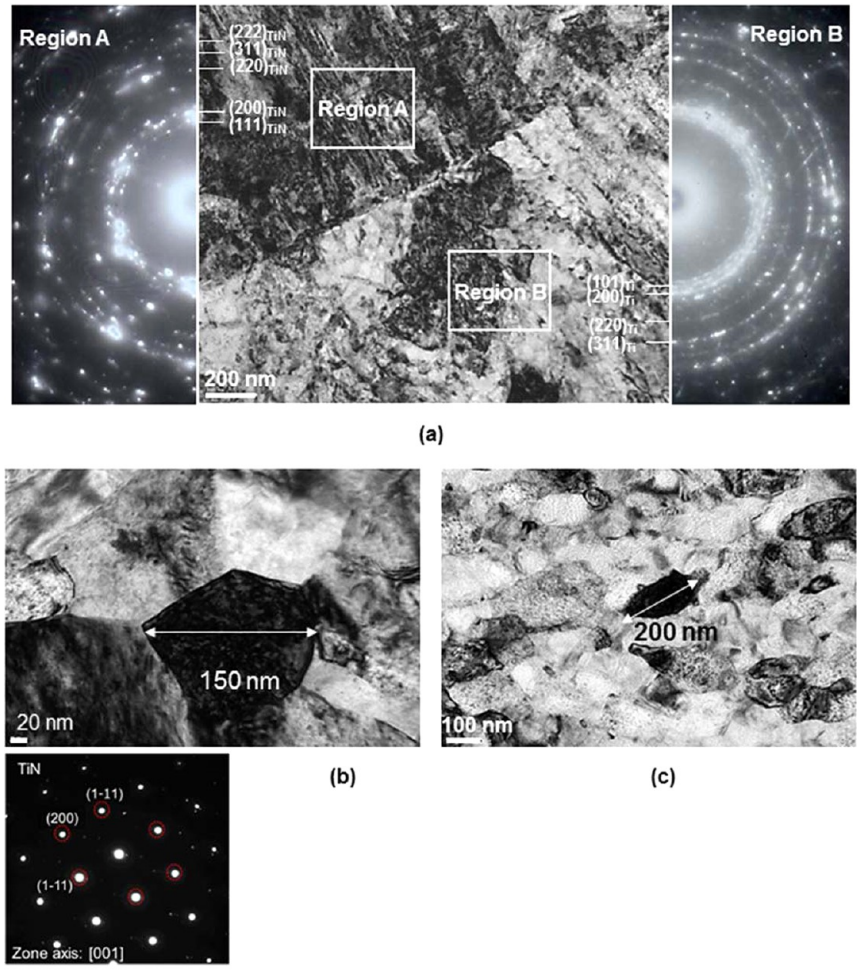

Figure 7. (a) HR TEM image and SADP of the interface and adjacent materials of Type 2, (b) a nano size grain of TiN layers in Type 2 and the SADP from the grain, (c) a nano size grain of TiN layers in Type 3.

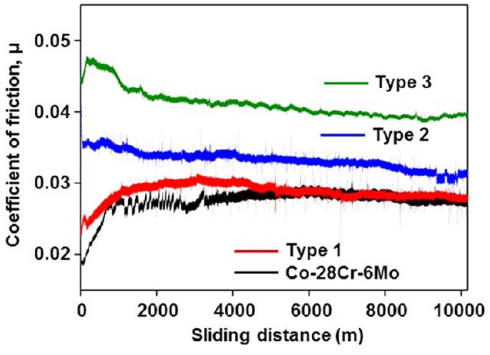

Figure 8. Friction coefficient with increasing sliding distance.

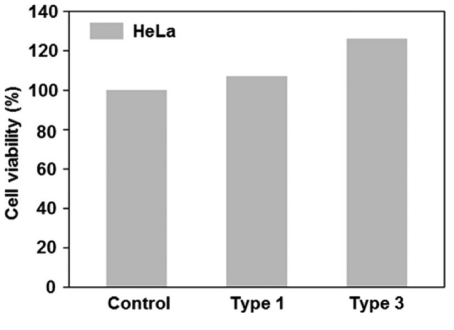

Figure 9. Biocompatibility test results for Types 1 and 3 coatings.

and the disk.[23] Ultimately, the accumulation of denatured protein leads to more extensive formation of a protein film adhering to the disk and thus protects the UHMWPE-pin from wear.

Studies have shown that small pores worsen the lubricating conditions and multiply the direct metallic contacts in the friction zone.[21,21] According to Figures 4–6, both the pore size and density in Type 3 are greater than those in Type 2. However, more extensive experimental studies are required to determine the optimum distribution, size, and density of pores for optimal wear properties. The chemical analyses in Figures 5–7 also reveal that the coatings are free of oxides and other contaminants that may produce undesirable side effects during operation. Biocompatibility is a critical parameter for use as a medical device component material. Thus, the positive biocompatibility test results in Figure 9 indicate that the coatings produced in this study have great potential as bearing materials in THRs.

5. CONCLUSIONS

The aim of this study was to develop new Ti-based composite coatings with enhanced wear resistance against the UHMWPE liner. Using a plasma spraying technique in a controlled N_2 gas atmosphere, Ti-TiN composite coatings with a lamellar structure of alternating Ti and TiN could be produced, and

dx.doi.org/10.1021/am302452f | ACS Appl. Mater. Interfaces 2013, 5, 395–403

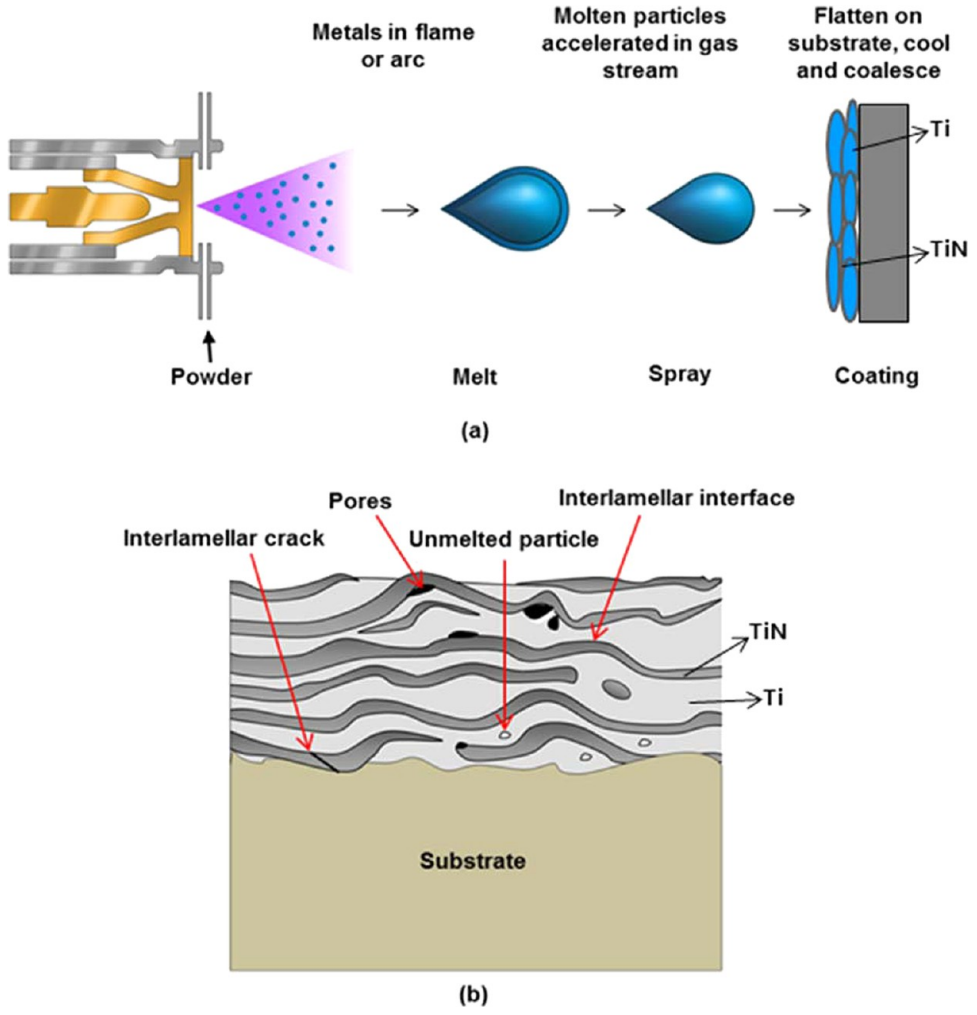

Figure 10. Schematic descriptions of (a) plasma-spraying process and (b) the cross-sectional microstructure of the Ti-TiN composite coatings.

the relative composition of Ti and TiN could be controlled. Because the composite coatings have mechanical properties intermediate between the properties of hard ceramic and tough metal materials, the combined wear properties and fracture toughness are improved as compared with pure metals and alloys, such as Ti and the Co-28Cr-6Mo alloy. The plasma-sprayed coatings generally have a porous structure that has previously been considered a disadvantage. However, our results clearly reveal that a certain level of porosity is highly beneficial to the friction and wear resistances by acting as a lubricant reservoir, and this porosity does not degrade the fracture resistance of the coatings. On the basis of both their biocompatibility test results and enhanced mechanical properties, the composite coatings developed in this study have great potential for use as bearing materials in THRs.

■ ASSOCIATED CONTENT

Ⓢ Supporting Information

The pictures of the plasma-spraying equipment and the coated samples for the wear test. This material is available free of charge via the Internet at http://pubs.acs.org.

■ AUTHOR INFORMATION

Corresponding Author

*E-mail: jwpark09@yonsei.ac.kr (J.-W.P.); chany@kist.re.kr (Y.C.K.). Phone: +82 221235834 (J.-W.P.); +82 29585457 (Y.C.K.). Fax: +82 221235834 (J.-W.P.); +82 29585449 (Y.C.K.).

Present Address

[§]Hyundai Welding Co., Ltd. in Pohang, Korea

Notes

The authors declare no competing financial interest.

■ ACKNOWLEDGMENTS

This study was supported by the Seoul R&BD program from Seoul Development Institute, Republic of Korea (SS100008), a grant from KIST, and a grant (M-2009-01-0014) from the Fundamental R&D Program for the Core Technology of Materials, which is funded by the Ministry of Knowledge Economy, South Korea. We also appreciate graduate students at Yonsei University, Mr. Jung-Hoon Kim and Mr. Ross E. Triambulo, for their technical support for this paper.

■ REFERENCES

(1) Geetha, M.; Singh, A. K.; Asokamani, R.; Gogia, A. K. *Prog. Mater. Sci.* **2009**, *54*, 397−425.
(2) Raimondi, M. T.; Pietrabissa, R. *Biomaterials* **2000**, *21*, 907−913.
(3) Ryan, G.; Pandit, A.; Apatsidis, D. P. *Biomaterials* **2006**, *27*, 2651−2670.
(4) Kanaga Karuppiah, K. S.; Bruck, A. L.; Sundararajan, S.; Wang, J.; Lin, Z.; Xu, Z. H.; Li, X. *Acta Biomater.* **2008**, *4*, 1401−1410.

(5) Hall, R. M.; Bankes, M. J. K.; Blunn, G. *Curr. Orthop.* **2001**, *15*, 281−290.
(6) Jin, Z. M.; Stone, M.; Ingham, E.; Fisher, J. *Curr. Orthop.* **2006**, *20*, 32−40.
(7) Garzino-Demo, G. A.; Lama, F. L. *Surf. Coat. Technol.* **1995**, *76*−*77*, 487−493.
(8) Galvin, A. L.; Williams, S.; Hatto, P.; Thompson, J.; Issac, G.; Stone, M.; Ingham, E.; Fisher, J. *Wear* **2005**, *259*, 972−976.
(9) Österle, W.; Djahanbakhsh, M.; Hartelt, M.; Wäsche, R. *Wear* **2008**, *265*, 1727−1733.
(10) Wang, A.; Essner, A.; Polineni, V. K.; Stark, C.; Dumbleton, J. H. *Tribol. Intl.* **1998**, *31*, 17−33.
(11) Niinomi, M. *Biomaterials* **2003**, *24*, 2673−2683.
(12) Torregrosa, F.; Barrallier, L.; Roux, L. *Thin Solid Films* **1995**, *266*, 245−253.
(13) Anttila, A.; Lappalainen, R.; Heinonen, H.; Santavirta, S.; Konttinen, Y. T. *New Diamond Frontier Carbon Technol.* **1999**, *9*, 283−288.
(14) Kim, E. H.; Kim, Y. C.; Han, S. H.; Yang, S. J.; Park, J. W.; Seok, H. K. *J. Kor. Inst. Met. Mater.* **2009**, *47*, 13−20.
(15) Hunt, J. A.; Callaghan, J. T.; Sutcliffe, C. J.; Morgan, R. H.; Halford, B.; Black, R. A. *Biomaterials* **2005**, *26*, 5890−5897.
(16) *ASTM Standard Test Method for Wear Testing of Polymeric Materials Used on Total Joint Prothesis*; ASTM International: West Conshohocken, PA, 2006; Vol. *F732*−*00*, pp 271−280.
(17) *Biological Evaluation of Medical Devices Part 1: Evaluation and Testing*; International Organization for Standardization: Geneva, 2003; Vol. *ISO 10993*−*5*.
(18) *Biological Evaluation of Medical Devices Part 5: Test for In vitro Cytotoxicity*; International Organization for Standardization: Geneva, 1999; Vol. *ISO 10993*−*5*.
(19) Irene, E. A. *Surfaces, Interfaces, aAnd Thin Films for Microelectronics*. John Wiley & Sons: New York, 2008.
(20) Sanmarchi, C.; Liu, H.; Lavernia, E. J.; Rangel, R. H.; Sickinger, A.; Muehlberger, E. *J. Mater. Sci.* **1993**, *28* (12), 3313−3321.
(21) Takadoum, J., *Material and Surface Engineering in Tribology*; John Wiley & Sons: New York, 2008.
(22) Gradzka-Dahlke, M.; Dabrowski, J. R.; Dabrowski, B. *Wear* **2007**, *263*, 1023−1029.
(23) Lu, Z.; McKellop, H.; Liao, P.; Benya, P. *J. Biomed. Mater. Res.* **1999**, *48*, 458−464.